# Belt Sprinkling Detection Method under Complex Working Conditions Based on Machine Vision

Wenzhu Wang, Shaochuan Xu, and Bo Cong

*Abstract*—Belt conveyors are extensively utilized in material transportation across metallurgy, mining and other industries. Their prolonged operation inevitably leads to issues such as belt deviation and spillage. Currently, belt deviation is primarily due to the uneven distribution of ore, which also contributes to spillage. If these issues are not promptly addressed, they can disrupt production and pose numerous safety risks. The ore transportation process is often characterized by heavy smoke and a complex environment, making manual inspections time-consuming, labor-intensive, and potentially hazardous. This paper introduces a machine vision-based belt sprinkling detection method for complex working conditions. It enhances and processes grayscale images of the belt, collected by a camera, to eliminate smoke interference and accentuate the features of the belt and ore. Edge detection and the Hough transform are employed to pinpoint the belt's edge, ascertaining the distribution of the belt and ore within it. A GWO-SVM (Grey Wolf Optimizer-Support Vector Machine) model is then constructed to predict the belt's operational state in real-time, identifying any anomalies to ensure safe production. Experimental comparisons demonstrate that the GWO-SVM model dynamically selects optimal parameters for 'c' and 'g', yielding accurate classification and detection results. It is characterized by high precision, robust real-time performance, and excellent stability, effectively achieving cost savings and safeguarding production safety.

*Index Terms*—Belt conveyor; Image processing; GWO-SVM; Sprinkling detection

## I. INTRODUCTION

The belt conveyor is composed of a belt, a driving drum, a reversing drum and an idler, which has a simple structure and relies on the friction between the drum and the belt to realize the function of transporting ore. Belt conveyor has the characteristics of large transportation volume, long transportation distance, uphill and downhill transmission and sustainable transportation, so it has great advantages in the transportation of granular and powdery items, and has been widely used in the transportation of major ores. Therefore, the performance and working condition of the belt conveyor are very important for the production of the factory. In the

Wenzhu Wang is a Teaching assistant of School of Information Technology, Changchun Technical University of Automobile, Changchun, 130013 China. (e-mail: w1599751883@163.com).

Shaochuan Xu is a Professor of School of Electronic and Information Engineering, University of Science and Technology Liaoning, Anshan, 114051 China. (Corresponding author, phone: 86-0412-5929747; e-mail: shaochuanxu1@163.com).

Bo Cong is a Teaching assistant of School of Electrical Engineering, Changchun Technical University of Automobile, Changchun, 130013 China. (e-mail: simon202408@163.com).

process of equipment installation and use, due to the different forces in various parts of the belt and the uneven placement of materials, the belt conveyor is prone to the problem of belt sprinkling, which will reduce the work efficiency; If the material falls into the equipment, there is a risk of damaging the equipment, bringing unnecessary economic losses, and also bringing safety hazards to the staff. Moreover, the belt sprinkling shows that the boredom on the belt is unevenly distributed, which is very easy to cause the belt to deviate and fail, and then cause more fault problems [1]. Therefore, it is necessary to detect the sprinkling phenomenon of the belt conveyor in time. At present, the fault detection of belt conveyor mostly depends on manual work, because the belt conveyor working range is larger, the distance is longer, the quantity is excessive, such workload needs a large amount of labor, the cost is expensive, and the factory environment is more complex, the influence of smoke is larger, and the danger factor is higher. In summary, it is necessary to design a method to detect whether there is a risk of spilling in the belt conveyor.

Guo Xiaoqiang and Liu Xinhua conducted some research on the problem of the imbalance of data obtained from the inspection images of the belt conveyor, and analyzed the characteristics and data of the fault-like characteristics [2]. Li Weiwei, and Li Chunqing proposed a computer vision detection algorithm based on multiple groups of lasers, which accurately segmented the laser fringe area through image processing and analysis, accurately located the tear area of the conveyor belt, and supported the user-defined alarm level of tear detection, which has a wider range of applications [3]. Zhu Liang, Li Dongbo and Wu Chongyou et al. used regression analysis methods such as SVM and Extreme Learning Machine (ELM) to establish an online prediction model of belt bias using the deviation features extracted by LTSA+GRNN and CDBN as inputs, and the experimental results were considerable [4]. Wang et al. presented an Audio-Visual Fusion technique to detect conveyor belt longitudinal tears, improving upon single-modal methods [5]. Leite et al. conducted experiments on the test bench equipped with conveyor belts and laser scanners, which proved the effectiveness of three detection algorithms: Three Sigma, Cumulative Sum Control Chart (CUSUM), and Truncated Exact Linear Time [6].

Nevertheless, it can be observed that the preponderant part of the current research is predominantly focused on the detection of large-scale malfunctions such as belt tearing and belt rupture. There is a paucity of in-depth discussion regarding the potentially significant impact that belt spillage might have on the deviation of the belt conveyor. However, research on spillage detection is of great significance.

Spillage not only leads to material waste and environmental pollution but also may cause hidden safety hazards and affect the normal operation and service life of the conveyor system. It can help improve the overall operational efficiency and reliability of the conveyor belt system, reduce maintenance costs and potential accidents, and ensure the sustainable and stable progress of industrial production.

Combined with the complex working environment of the belt conveyor, this paper proposes a belt sprinkling detection method based on machine vision, which can accurately determine whether the belt has the risk of spilling in complex environments such as hazy smoke and light shortage, so as to prompt the staff to correct it in time and avoid greater faults caused by uneven material distribution. In this paper, the Retinex image enhancement algorithm is used to remove smoke interference from the image, and then the image is grayscale and filtered to highlight the characteristics of the belt and the material. Then, the Canny operator edge extraction algorithm combined with the Hough transform straight line was used to detect and locate the edge position of the belt, so as to further obtain the material distribution information on the belt. Then, a cross-sectional line is drawn on the belt using the coordinates of the edge line segment of the belt, and the gray value of each pixel on each line segment is used to form a "new cross-section". Then, the GWO-SVM sprinkling prediction model trained by the corresponding data is used to judge whether the belt has a spilling risk, and the corresponding early warning is given based on the detection results of multiple images.

## II. SITUATION ANALYSIS AND DETECTION METHOD COMPOSITION

### A. Situation Analysis

In the process of using the belt conveyor to transport the material, there is often a situation that the material on the belt falls and the material is spilled in a large area, if it cannot be found in time, the material falls between the belt and the roller, and the friction with the belt is easy to scratch the belt, and then causes the occurrence of belt tearing fault. In addition, the occurrence of material spilling means that the material is distributed unevenly on the belt with a high probability, due to the existence of gravity, if it cannot be adjusted in time, it is easy to cause the belt to one side to deviate, that is, the belt deviation phenomenon, as shown in Fig. 1. From the perspective of on-site work, due to the long working distance of the belt conveyor, the fallen materials are not easy to recover, and the smoke and dust on site are large, which will bring certain safety hazards to the staff [7]. Furthermore, it can be found that it is necessary to detect whether there is a risk of spilling materials on the belt to detect the distribution status of the material and prevent belt deviation and belt tearing failure [8]. To a certain extent, timely intervention in the occurrence of belt sprinkling can effectively extend the service life of the belt conveyor, and at the same time ensure the efficient and safe production of the factory.
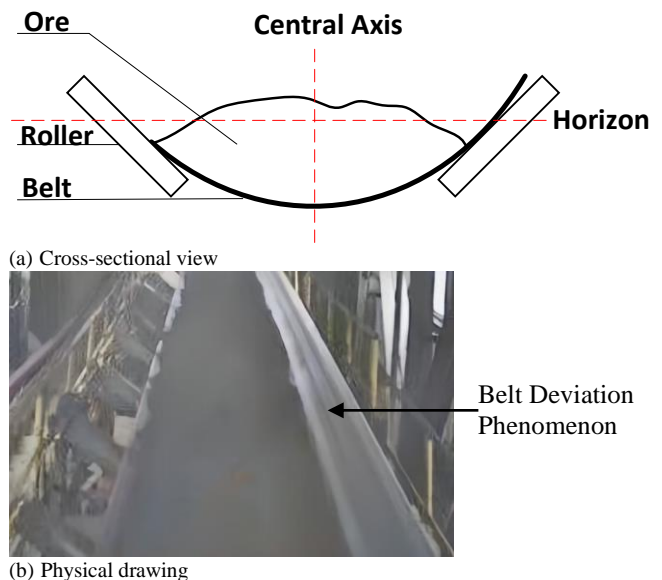


(a) Cross-sectional view



(b) Physical drawing
Fig. 1. Uneven material distribution

### B. Composition of The Assay Method

The first step of the inspection is to install a professional camera in a suitable position directly above the belt conveyor, so that it is easy to capture the video of the belt conveyor when it is working, and capture the image from the captured real-time video. The working environment of the coal mining plant is relatively harsh, and it is inevitable that smoke and dust will be dispersed into the environment during the ore transportation process, and some smoke and dust will also be adsorbed on the camera. Therefore, the image enhancement algorithm is combined to highlight the characteristics of the belt and ore, and then the image is grayscale and filtered, which can remove impurities and retain effective information to a large extent. Then, the edge detection operator and Hough transform are combined to locate the edge position of the belt in the selected ROI region. A cross-sectional line containing belt and ore information is drawn on the image-processed belt image by referring to the coordinates of the belt edge position. The information of each pixel on this section line is used to remove the excess part, and the feature information is retained to form a "new cross-section", and the data of each pixel on the "new cross-section" is used to train the GWO-SVM sprinkling detection model. After that, the model is used to make corresponding early warnings on whether there is a risk of spilling on the belt, and the staff can grasp the operation status of the belt through the early warning information, so as to reduce economic losses and ensure safe production.

The steps of the sprinkler detection method studied in this paper include: image acquisition, image processing, positioning the coordinates of the edge of the belt, obtaining the characteristic information of the belt and the ore, and using the sprinkler detection model to judge whether there is a risk of sprinkling. Image acquisition is to take a screenshot of the real-time video captured by the camera as an image; Image processing is to do image enhancement, grayscale and filtering of the intercepted image, so as to reduce the noise interference in the smoke situation, so that the characteristics of the belt and the ore contained in it are more prominent; Locate the coordinates of the edge of the belt to prepare for obtaining the characteristic information of the belt and the ore,

use the information on the obtained cross-section to train the sprinkler detection model, and then the trained model can be used to make an early warning of the belt sprinkling. The specific steps are shown in Fig. 2.
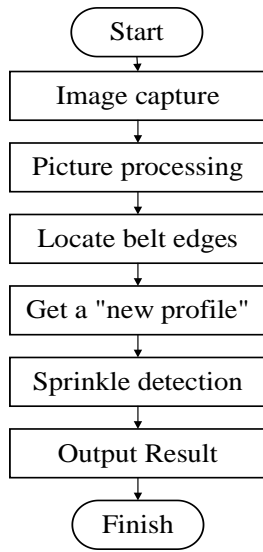
```
        Start
          │
    Image capture
          │
   Picture processing
          │
   Locate belt edges
          │
   Get a "new profile"
          │
   Sprinkle detection
          │
    Output Result
          │
        Finish
```

Fig. 2. Flow chart of the detection method

### III. Image Acquisition And Processing

#### A. Image Acquisition and Image Enhancement

Images are captured at intervals in the video obtained by the cameras installed in the field for subsequent image processing. The working place of the belt conveyor is mostly in the mine and processing site, the environment is relatively complex, and there are many interferences such as light noise, dust and smoke, and the working conditions are extremely complex. Therefore, the quality of the obtained images is good and bad, and if it is not processed in time, these interferences will affect the accuracy of subsequent detection results. For some low-contrast raw images, a suitable image enhancement algorithm can weaken the useless information and improve the contrast of the image. After many comparisons, it is found that the overall image quality and clarity of the image processed by the image enhancement algorithm are significantly improved compared with the unprocessed image, and the characteristics of the ore are more obvious, and the edge of the belt is clearer.

At present, the commonly used image enhancement algorithm is histogram equalization. Histogram equalization equalizes the three channels of color images R, G, and B respectively and then merges them, which is prone to problems such as uneven color and distortion, so it is mostly used for contrast enhancement of grayscale images. However, in this paper, the color image needs to be enhanced, and the image effect after histogram equalization is not very ideal. Although the characteristics of the ore area and the belt area on the belt are well displayed in the histogram equalization process, the contrast of the useful signal is reduced, which directly leads to some weak spots in the image becoming very obvious after processing, and the smoke interference cannot be well removed.

The Retinex algorithm is an image of the reflection properties that retains the essence of the object by removing or reducing the influence of incident information in the original image [9]. Among them, Multi-Scale Retinex (MSR) is developed on the basis of Single Scale Retinex (SSR), which can maintain the high fidelity of the image while reasonably compressing the dynamic range of the image [10]. Not only that, MSR can also achieve color enhancement, color constancy, local dynamic range compression, and global dynamic range compression of images [11]. Therefore, in this paper, the advanced version of the algorithm Multi-Scale Retinex in Retinex is used to enhance the original image. The calculation principle of the MSR image enhancement algorithm is as follows:

$$R(x,y) = \sum_{k}^{K} w_k (\log S_i(x,y) - \log(S_i(x,y) * G_n(x,y))) \tag{1}$$

Where S is the input; G is the filter function; K is the number of scales; w is the weight of each scale, which is generally $1/K$; R represents the output image of the logarithmic field [12].

After MSR image enhancement processing, the interference of smoke in the field environment can be greatly reduced, and the characteristics of ore and belt on the belt can be greatly improved, so that the contrast can be enhanced. Although the Retinex algorithm increases some of the noise, the image can be processed in subsequent work with little impact.

#### B. Image Grayscale and Filtering

The image after image enhancement is grayscaled, and the color image is converted into a grayscale image, saving the subsequent operation time, and highlighting the characteristics of the belt and the ore in which it is located [13]. There are many methods of grayscale image grayscale, and after many attempts to compare the results, it is found that the edge of the belt is the most obvious and clearest in the effect obtained by the weighted average method, and the characteristic information of the ore on the belt is greatly retained [14]. The weighted average method is to average the three components of R (red), G (green) and B (blue) in the RGB model with different weights:

$$Gray(i,j) = 0.299R(i,j) + 0.578G(i,j) + 0.114B(i,j) \tag{2}$$

Where R, G, and B represent the red, green, and blue components, respectively [15].

At this time, the flatness between the individual pixels on the obtained image is still not high enough, so it is necessary to filter the image. Considering the complexity of the on-site environment, the smoke and dust are dispersed in the environment from time to time, and the commonly used basic filtering method cannot meet the requirements well. After several comparison attempts, it is found that the bilateral filter considers both the spatial weight and the similarity weight when calculating the center pixel [16]. The spatial weight is used for denoising, and the similarity weight is responsible for protecting the edge, which can protect the effective information of the belt edge to the greatest extent and lay the foundation for the subsequent positioning of the belt edge position [17]. The results of the bilateral filter are:

$$BF = \frac{1}{W_q} \sum_{p \in S} G_s(p) G_r(p) * I_p \tag{3}$$

Where $G_r$ is the weight of the pixel value and $G_s$ is the weight of the spatial distance.

$$G_s = \exp(-\frac{\|p-q\|^2}{2\sigma_s^2})$$

$$G_r = \exp(-\frac{\|I_p - I_q\|^2}{2\sigma_r^2}) \tag{4}$$

Where $W_q$ is the sum of the weights of the pixel values of each pixel in the filter window, which is used for the normalization of the weights:

$$W_q = \sum_{p \in S} G_s(p)G_r(p) \tag{5}$$

After grayscale and bilateral filtering, the contrast of the obtained image is significantly improved compared with the original image. And while removing noise, the basic characteristics of the belt edge and the ore contained in the belt are retained. This set of image processing scheme is well adapted to the complex working conditions of the belt conveyor, which can greatly reduce the deviation of the detection results caused by the lack of clarity of the captured image caused by the smoke dispersion in the narrow environment and the coal ash attached to the lens.

## IV. LOCATE THE BELT EDGE POSITION

The result is a sharper image with more pronounced contrast. To detect whether there is a risk of spillage on a belt, the first step is to obtain the edge position of the belt. In order to better locate the edge position of the belt and reduce the amount of data and reduce the subsequent operation time, it is first necessary to perform edge detection on the entire content of the image, which can also delete some information that is weakly related to the experiment. The working principle of the edge detection operator is to first detect some pixels of the image outline and connect them, and then detect and supplement some boundary points that have not been detected, and at the same time remove the false boundary points and retain the real boundary points to connect them to form the edges of the objects in the image. At present, there are many commonly used edge detection operators, and in the image of the working environment of the belt conveyor under complex working conditions, the Canny operator in the first-order operator performs the best in this paper, considering the calculation speed and detection accuracy of each operator [18]. The Canny operator proposes a high-order threshold method of non-maximum suppression of the edge gradient direction and a high-order threshold method with double threshold, which can identify the edge of the image more accurately, and the edge of the complete belt is well detected in the experimental link in this paper.

The general outline of the object in the image is obtained through edge detection, but at this time, there is a lot of background information on the image that is not related to the subsequent sprinkling detection, such as windows, other equipment on the ground, etc., in addition to the belt conveyor and the ore on it. In order to save the calculation time, improve the calculation speed, and further ensure the accuracy of the positioning of the edge position of the belt, the region of interest (ROI) region is selected in a rectangular shape at the appropriate position on the image, and then the

Hough Transform is used to detect the straight line in the ROI area, and then the edge position of the belt is determined. Hough transform can identify geometric shapes in images, such as straight lines, circles, etc., and is a commonly used feature extraction method in image processing [19]. Combined with the site conditions studied in this paper, the ROI area was selected near the belt edge roller. The principle of Hough Transform detecting straight lines is: A straight line is determined by two points $A = (X_1, Y_1)$ and $B = (X_2, Y_2)$ in a Cartesian coordinate system, and the expression $y=kx+q$ is converted to a Hough space with respect to $(k,q)$ as:

$$\begin{cases} q = -kx_1 + y_1 \\ q = -kx_2 + y_2 \end{cases} \tag{6}$$

After the operation of the above method, the exact position of the edge of the belt can be obtained, as shown in Fig. 3.
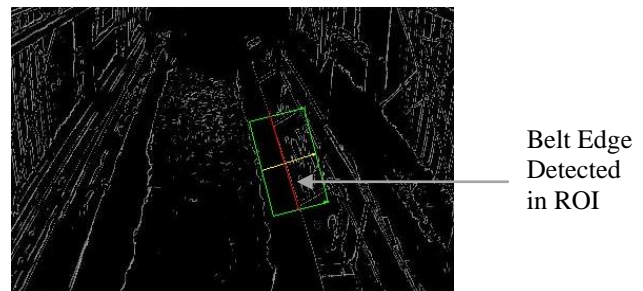


Belt Edge Detected in ROI

Fig. 3. The position of the edge of the belt that is positioned

Then, according to the different characteristics of the belt and the surrounding environment, combined with the huge difference in the gray value between the two, the line segment detected by the Canny operator combined with the Hough transform in the ROI is verified to be the required target line segment. If it is determined that the segment is the target segment, proceed to the next step, otherwise start again. In this way, the purpose of accurately positioning the position of the belt edge is realized, and the accuracy of the basic information of the belt and the mineral material contained in the belt is ensured by using the belt edge in the subsequently, so as to ensure the accuracy of the sprinkling material detection.

To validate the effectiveness of the edge localization algorithm proposed in this paper, an additional four edge detection operators were selected to combine with the Hough Transform and verification method, and the same set of 100 belt images was used to detect the left edge of the belt. Subsequently, the five sets of data were comprehensively compared and analyzed using accuracy and precision as evaluation metrics. The detection results are shown in TABLE I.

TABLE I
DETECTION RESULTS OF EDGE OPERATOR-HOUGH-VERIFICATION METHOD

| Method | Accuracy | Precision |
|---|---|---|
| Roberts-hough- verify | 90% | 94.44% |
| Prewitt-hough- verify | 84% | 93.02% |
| Sobel-hough- verify | 87% | 92.31% |
| Laplacian-hough- verify | 93% | 94.62% |
| Canny-hough- verify | 96% | 96.74% |

The comparative results of several experiments were analyzed, based on the dual consideration of accuracy and precision, the Canny operator and Hough transform combined with the verification method have good performance in accuracy and precision, and can accurately locate the edge position of the belt. Therefore, this method is used to locate the coordinate information on both sides of the belt in the ROI area, so as to accurately obtain the position information of the belt edge and ensure the follow-up work.

## V. ESTABLISHMENT OF GWO-SVM SPRINKLER DETECTION MODEL

### A. Data Processing

By positioning the edge positions on both sides of the belt, two-line segments representing the edge of the belt can be obtained within the ROI on both sides of the belt. Using the coordinate positions of the endpoints of these two-line segments, you can obtain the coordinates of the midpoints of the two-line segments. The principle is that the coordinates of the two points are $A = (X_1, Y_1)$ and $B = (X_2, Y_2)$ respectively, so the coordinates of the midpoint of the two points are:

$$C = (\frac{X_1 + X_2}{2}, \frac{Y_1 + Y_2}{2}) \qquad (7)$$

From this, the position coordinates E and F of the midpoint on the relevant line segment of the edge position on both sides of the belt can be obtained, respectively. Taking these two points as the two endpoints of a new line segment, a line segment EF perpendicular to the running direction of the belt conveyor is drawn in the filtered grayscale image, as shown in Fig. 4. By drawing this cross-section on the image, you can get the grayscale value corresponding to each pixel on the cross-section. This string of data contains the basic information of the belt and the ore contained in it within a certain range, as well as the distribution state of the material on the belt. Through this data and the corresponding picture, the working state of the belt conveyor at that moment can be obtained.
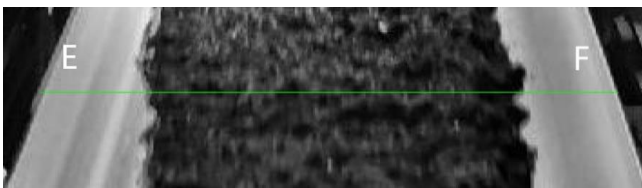


Fig. 4. Drawn cross-section

By mapping the pixel value corresponding to each pixel on the image to the Cartesian coordinate system, a cross-sectional diagram of the distribution state of the material on the belt at that moment can be obtained. Combined with the pictures corresponding to the data of each section, and then analyzing the distribution state of the materials on the belt, the working state on the belt can be roughly divided into: normal state and sprinkling state. Among them, the sprinkler state can be subdivided into three forms: left-side sprinkler, right-sided sprinkler and two-sided sprinkler. They are shown in Fig. 5.
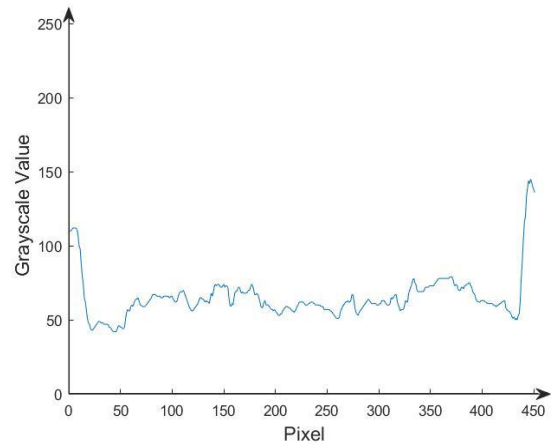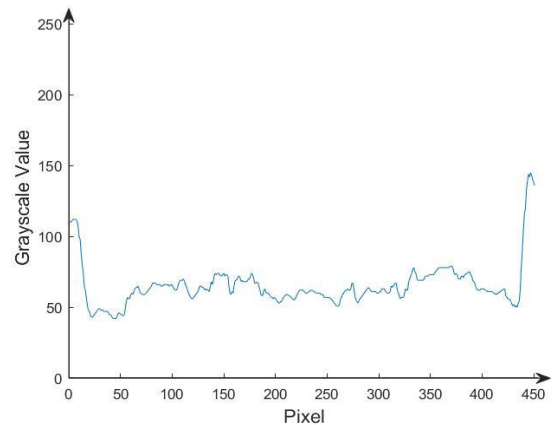


(a) Normal state
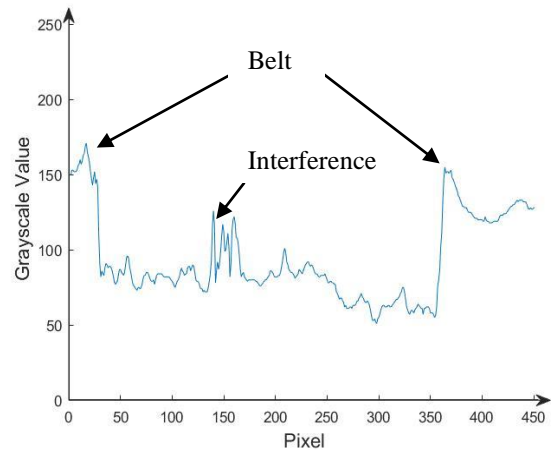


(b) Sprinkle on the left side
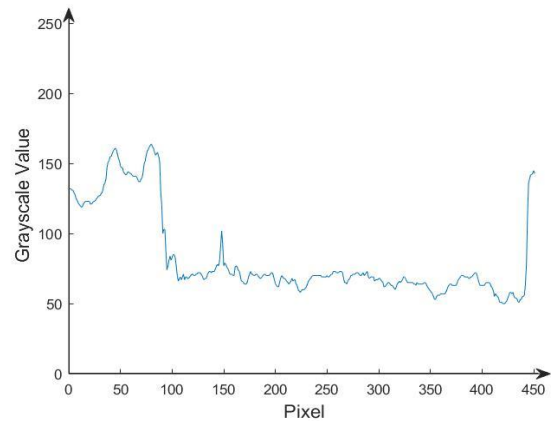


(c) Sprinkle on the right side



(d) Sprinkle on both sides

Fig. 5. Cross-section diagram of the target line segment

During the operation of the belt, due to the different quality of the material itself, the belt will be deformed. In addition, it may also cause certain changes in the image during the image acquisition process. These variations may result in different cross-section lengths acquired on images at different moments. Combined with the data analysis, it is found that the main evidence for judging whether there is a risk of spilling in the belt is the gray value of the pixels near both sides of the belt. So, $N_L$ pixels were selected from the left and $N_R$ pixels from the center to the right side of the belt to form a "new cross-section" with the number of $N_L+N_R$. Some of the redundancy of the processed data is removed, which can improve the computing speed.

Through the analysis of the belt image and its corresponding section map, it is found that due to the scratches on the belt, coal dust residue, ore reflection and other factors, some areas in the target section will have some pixel gray values will be relatively large. Therefore, the traditional threshold method has weak anti-interference performance.

### B. GWO-SVM Sprinkler Detection Model

According to the need, the classification results of the model are divided into two categories: with spillage risk and no spillage risk. This is a strict binary classification problem, and support vector machine (SVM) is one of the typical classification algorithms in machine learning. It performs well in solving small-sample, nonlinear and high-dimensional pattern recognition, but the sum selection of parameters $c$ and $g$ in SVM has a great impact on the overall classification effect, and it is a great task to manually modify and find suitable parameter values in the sprinkler classification model. Grey Wolf Optimizer (GWO) is a swarm intelligence optimization algorithm with simple structure and strong convergence, so the sprinkler detection model in this paper uses the grey wolf algorithm to optimize the parameters c and g in the SVM algorithm, and establishes the "GWO-SVM sprinkler detection model".

Support vector machine is a typical classification model in machine learning. The main idea is to find a hyperplane that separates two different classes of samples [20]. The sample set is given $D\{(x_1, y_1), (x_2, y_2),...,(x_m, y_m)\}$ , $x_i \in R^n$ , $y_i \in \{-1, +1\}$, $i = 1, 2, ..., m$. In the current sample space, the hyperplane can be represented as:

$$w \cdot x + b = 0 \tag{8}$$

Where $w = (w_1; w_1; \cdots; w_d)$ is the normal vector of the hyperplane; $b$ is the displacement term. The distance from any point $x$ in the sample to the hyperplane $(w,b)$ is $\gamma = \frac{|w^T x + b|}{\|w\|}$, which is obtained according to the Lagrangian operator:

$$\max_{\alpha} \quad \sum_{i=1}^{m} \alpha_i - \frac{1}{2} \sum_{i=1}^{m} \sum_{j=1}^{m} \alpha_i \alpha_j y_i y_j x_i^T x_j$$
$$s.t. \quad \sum_{i=1}^{m} \alpha_i y_i = 0, \ \alpha_i \geq 0, \quad i = 1, 2, \cdots, m \tag{9}$$

Where $\alpha_i$ is a Lagrangian operator. In practice, there are very few cases where it is completely linearly separable. To address overfitting, SVMs introduce "soft intervals", which allow a small percentage of samples to not satisfy the constraint. and the introduction of the "relaxation variable" $\xi_i \geq 0$, obtained

$$\min_{w, b, \xi_i} \frac{1}{2} \|w\|^2 + C \sum_{i=1}^{m} \xi_i \tag{10}$$

For the input is given the training sample set $D$, the kernel function $\kappa(x, z)$ and the penalty factor $C$ are selected to construct and solve the convex quadratic programming problem:

$$\min_{\alpha} \quad \frac{1}{2} \sum_{i=1}^{m} \sum_{j=1}^{m} \alpha_i \alpha_j y_i y_j \kappa(x_i, x_j) - \sum_{i=1}^{m} \alpha_i$$
$$s.t. \quad \sum_{i=1}^{m} \alpha_i y_i = 0, \ 0 \leq \alpha_i \leq C, \quad i = 1, 2, \cdots, m \tag{11}$$

The optimal solution is obtained, and then the classification decision function is obtained:

$$f(x) = sign(\sum_{j=1}^{m} \alpha_i^* y_i \kappa(x_i, x_j) + b^*) \tag{12}$$

GWO classifies the gray wolf population into four classes: $\alpha$, $\beta$, $\gamma$, and $\omega$. The group leader is the gray wolf ($\alpha$) who is responsible for leading the search direction and influencing other gray wolves through their own behavior and position; Individuals of the second level ($\beta$) have higher adaptability but less than $\alpha$, and will be affected by $\alpha$, and adjust their position and behavior by interacting with $\alpha$. The third-level gray wolf individuals ($\delta$) will be affected by $\alpha$ and $\beta$, and adjust their position and behavior through interaction with $\alpha$ and $\beta$, and the $\alpha$ and $\beta$ with poor adaptability will be reduced to $\delta$. The gray wolf with the lowest fitness value ($\omega$) is the lowest level individual, and in the search process, it mainly adjusts its position and behavior through interaction with other gray wolves, and the omega wolf follows the $\alpha$, $\beta$, and $\delta$ wolves to track and round up, and the position of the prey is the optimal solution of the objective function [21]. First, the gray wolf surrounds the prey:

$$\vec{D} = \left| \vec{C} \cdot \vec{X}_p(t) - \vec{X}(t) \right|$$
$$\vec{X}(t+1) = \vec{X}_p(t) - \vec{A}(t) \cdot \vec{D} \tag{13}$$

Where $\vec{X}_p(t)$ is the position vector of the prey, $\vec{X}(t)$ is the position vector of the gray wolf, $\vec{D}$ is the distance between the gray wolf and the prey, and $\vec{X}(t+1)$ is the position update formula of the gray wolf according to the distance occurrence. The coefficients $\vec{A}$ and $\vec{C}$ are formulas for

$$\vec{A} = 2\vec{a} \cdot \vec{r_1} - \vec{a}$$
$$\vec{C} = 2 \cdot \vec{r_2} \tag{14}$$

Where $a$ is the convergence factor, which decreases linearly from 2 to 0 with the increase of the number of iterations, and $\vec{r_1}, \vec{r_2}$ is a random number within [0,1].

Using the location of the $\alpha$, $\beta$, and $\delta$, update the location of all gray wolves to:

$$\begin{cases} \vec{D}_\alpha = \left| \vec{C}_1 \cdot \vec{X}_\alpha - \vec{X} \right| \\[2mm] \vec{D}_\beta = \left| \vec{C}_2 \cdot \vec{X}_\beta - \vec{X} \right| \\[2mm] \vec{D}_\delta = \left| \vec{C}_3 \cdot \vec{X}_\delta - \vec{X} \right| \end{cases} \quad (15)$$

Among them, $\vec{D}_\alpha$、$\vec{D}_\beta$、$\vec{D}_\delta$ is $\alpha$、$\beta$、$\delta$ distances from other wolves; $\vec{X}_\alpha$、$\vec{X}_\beta$、$\vec{X}_\delta$ is the position of $\alpha$、$\beta$、$\delta$ ; $\vec{C}_1$、$\vec{C}_2$、$\vec{C}_3$ is a random vector; $\vec{X}$ is the current location of the gray wolf.

$$\begin{cases} \vec{X}_1 = \left| \vec{X}_\alpha - A_1 \cdot \vec{D}_\alpha \right| \\[2mm] \vec{X}_2 = \left| \vec{X}_\beta - A_2 \cdot \vec{D}_\beta \right| \\[2mm] \vec{X}_3 = \left| \vec{X}_\delta - A_3 \cdot \vec{D}_\delta \right| \end{cases} \quad (16)$$

$$\vec{X}(t+1) = \frac{\vec{X}_1 + \vec{X}_2 + \vec{X}_3}{3}$$

Among them, $\vec{X}_1$、$\vec{X}_2$、$\vec{X}_3$ are the positions of gray wolves $\omega$ that need to be adjusted due to the influence of $\alpha$, $\beta$ and $\delta$ wolf packs. $\vec{X}(t+1)$ is the position vector of the gray wolf after the update, and $t$ represents the number of iterations. When hunting, a change in the convergence factor $\alpha$ causes a change in coefficient A, which passes |A| size to determine whether to find the prey location when |A|≤1, the wolves concentrate on attacking the prey position (local optimal solution). When |A|>1, the wolves move away from their prey and look for new prey (global search). The gray wolf looks for prey based on the position of the $\alpha$, $\beta$, and $\delta$, and then finds the global optimal solution [22].

In order to solve the problem that the penalty parameter c of the support vector machine and the width parameter g of the RBF basis function have an impact on the SVM classification results, the GWO algorithm is used to optimize the parameters globally. The objective function uses the best accuracy of the five-fold cross-validation. The objective function formula is as follows:

$$Fitness = \frac{n}{N} \times 100\% \quad (17)$$

Where $n$ is the number of samples that are accurately identified, and $N$ is the total number of samples identified. The greater the fitness, the higher the recognition accuracy of the optimization model.

The steps to build a GWO-SVM sprinkler model are as follows:

(1) The samples are divided into a training set and a test set, and normalized.

(2) Initialize it with GWO, and set algorithm parameters such as population number, maximum number of iterations, and optimization variable range.

(3) Using GWO, the maximum value of the objective function is used as the optimization goal to obtain the optimal parameters.

(4) The optimized SVM is tested by using the test set data.

(5) Output the test set classification results of GWO-SVM.

## VI. Model Classification Results And Analysis

The belt image data of different working conditions were selected to verify the GWO-SVM sprinkler detection model constructed in this paper. In this paper, 700 samples were selected for training. 300 samples were selected for testing, including 150 samples with no spilling risk and 150 samples with spilling risk.

Fig. 6 presents the "Actual classification and predictive classification graphs of training sets," showcasing a comparative analysis between the actual and predicted classifications within our training dataset. The y-axis, labeled "Actual classification," ranges from 1 to 2. The x-axis represents the sample indices, spanning from 0 to 350, with marked intervals at 50, 100, 150, 200, 250, 300, and 350. The chart demonstrates the model's performance, with an impressive accuracy of 100%, as indicated by the annotation "Accuracy= 100%."
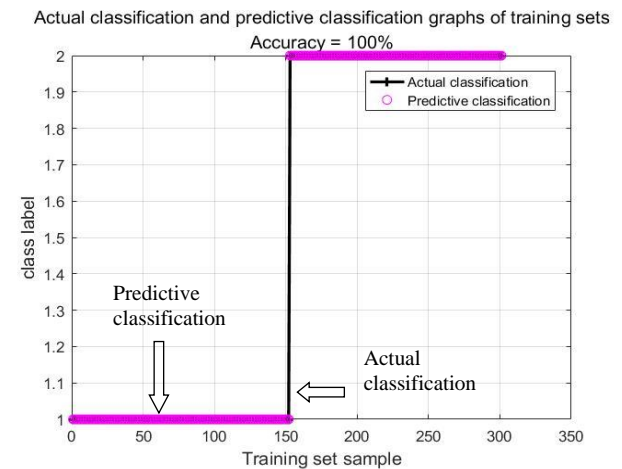


Fig. 6. Training set classification results of GWO-SVM model

The depicted graph illustrates an exemplary case of model accuracy, where the predictive classifications align perfectly with the actual classifications across the training set. This perfect alignment is reflected in the data points, which, due to the 100% accuracy, indicating that the model's predictions match the actual values without deviation. Such a result is indicative of an ideal scenario where the model has learned the training data patterns with precision, suggesting a high degree of generalization potential within the confines of the training dataset.

Fig.7 depicts the "Fitness curve Accuracy [GWO method]," which traces the optimization progress of the Grey Wolf Optimizer (GWO) algorithm across multiple iterations. The chart displays two lines: "Optimum fitness" and "Mean fitness," showcasing the best and average fitness values achieved by the GWO method. The model achieves 100%

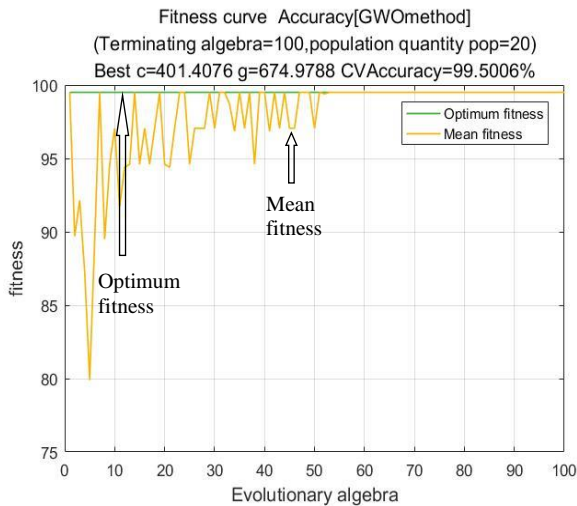accuracy on the test set when c is 401.4076 and g is 674.9788, which corresponds to the highest accuracy.



Fig. 7. Fitness curve

The fitness curve in Fig. 7 illustrates the convergence behavior, with the "Optimum fitness" line rapidly ascending towards the maximum fitness value, indicating the algorithm's effectiveness in locating the optimal solution. The "Mean fitness" line also shows a steady increase, demonstrating the overall improvement in the population's fitness over the course of the evolutionary process. The GWO method with a population size of 20, converges to an optimal fitness value for the SVM at the 100th iteration, suggesting a robust search capability and efficient exploration of the solution space. The high cross-validation accuracy of 99.5006% indicates that the model derived from the GWO algorithm generalizes well to unseen data, which is a critical aspect of model validation. This high accuracy is a testament to the algorithm's ability to find solutions that not only perform well on the training data but also maintain high predictive power on new, independent datasets.

Fig. 8 shows the test set classification results of the GWO-SVM sprinkler detection model, which juxtaposes the actual class labels with the predictions made by our model on the test dataset. The chart is marked with an impressive accuracy of "98.9967%," indicating the proportion of correctly classified instances.
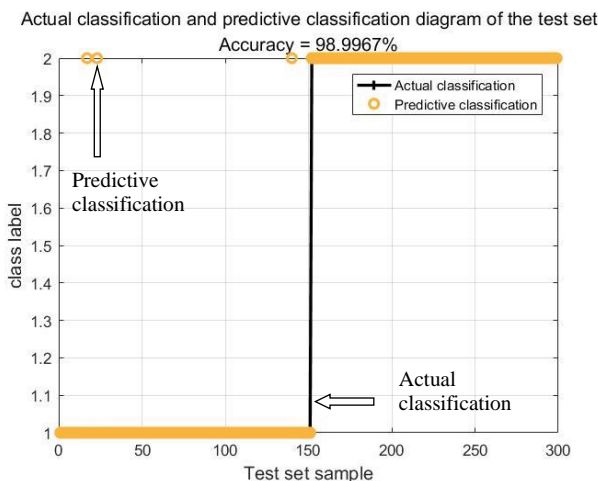


Fig. 8. Test set classification results of GWO-SVM model

The diagram in Fig. 8 vividly demonstrates the alignment between the model's predictions and the actual class labels for the test set samples. With a high accuracy of 98.9967%, the model exhibits a strong predictive capability, suggesting that it has learned the underlying patterns of the data effectively. The close proximity of the "Actual classification" and "Predictive classification" lines across the majority of the samples indicates a high degree of consistency between the model's predictions and the true labels.

The GWO-SVM sprinkler detection model was compared with the SVM sprinkler detection model and BP neural network. In order to ensure that the results can obtain the average performance of each model of the algorithm, each group of experiments was run independently for 10 times, and the average value of the recognition accuracy was taken. The population size of the GWO-SVM sprinkler detection model is N=20, and the maximum number of iterations $t_{max}$=100 is set. TABLE II shows the test results.

After comparison, it is found that the GWO-SVM sprinkler detection model proposed in this paper and the BP neural network have excellent performance, but the BP neural network takes a long time, which is not conducive to the real-time monitoring of the actual site. However, the GWO-SVM sprinkler detection model proposed in this paper takes a short time and is not inferior to the BP neural network, which is very suitable for real-time monitoring. In addition, the GWO-SVM sprinkler detection model dynamically selects the appropriate parameters c and g, which greatly improves the classification effect of SVM, eliminates the uncertainty of the SVM sprinkler detection model relying on human experience to select parameters, and plays a role in feature dimensionality reduction, reasonably avoids the problem of dimensionality disaster, and improves the performance of the model. The excellent performance results proved the effectiveness of the sprinkler detection model.

TABLE II
SPRINKLER DETECTION RESULTS OF DIFFERENT ALGORITHMS

| Method | Number of test samples | Recognition accuracy | Precision | Time/s |
|---|---|---|---|---|
| SVM sprinkler detection model | 300 | 96.67% | 96.67% | 6.9 |
| GWO-SVM sprinkler detection model | 300 | 99.00% | 98.68% | 8.2 |
| BP Neural Network | 300 | 99.33% | 99.33% | 22.4 |

## VII. CONCLUSION

In this paper, we propose a belt sprinkler detection method for complex working conditions that integrates image enhancement, edge detection, Hough transform, GWO, and SVM algorithms. To address the challenging environment at the actual site, where heavy smoke can impede detection results, we have incorporated the MSR image enhancement algorithm. This approach effectively mitigates the impact of smoke and enhances the detection accuracy.

By leveraging the distinct characteristics of ore and the belt on the conveyor, our method enables real-time assessment of the risk of spillage in the current state of the belt conveyor. Extensive experimental results demonstrate that our proposed method boasts high accuracy, robust stability, and excellent real-time performance. It can effectively prevent belt sprinkling incidents, thereby averting a cascade of failures that can arise from uneven ore distribution on the belt. Overall, the sprinkler detection algorithm presented in this paper excels in diagnostic precision and generalization capability, offering significant practical value.

Future research should focus on integrating deep learning with SVM to enhance performance, optimizing image enhancement algorithms for low-light conditions, and investigating multi-sensor fusion systems for robustness against corrupted sensor signals and synchronization errors.

## REFERENCES

[1] Nguyen Vanliem, Feng Dapeng, and Hou Lang, "Study on running deviation mechanism and intelligent control of belt conveyor," Vibroengineering PROCEDIA, vol. 36, pp.6, 2021.

[2] Xiaoqiang G, Xinhua L, and Hao Z, "Belt Tear Detection for Coal Mining Conveyors," Micromachines, vol. 13, no.3, 2022.

[3] Weiwei L, Chunqing L, and Fanlei Y, "Research on belt tear detection algorithm based on multiple sets of laser line assistance," Measurement, 2021.

[4] Chu Q Y, Meng G Y, and Fan X, "Analysis of Speed and Belt Deviation of the Conveyor Belt," Advanced Materials Research, vol. 1453, pp.339-339, 2011.

[5] Wang Y, Du Y, Miao C, Miao D, Zheng Y and Yang D, "Longitudinal tear detection method for conveyor belt based on multi-mode fusion." Wireless Networks, vol. 30, no.4, pp.2839-2854, 2024.

[6] Leite J R, Cavalieri D C, and Prado A R, "Efficient monitoring of longitudinal tears in conveyor belts using 2D laser scanner and statistical methods." Measurement, vol. 227, pp.114225, 2024.

[7] Mozib E F, Zhang N, and Peterson D, "Weed Detection Using Color Machine Vision," Transactions of the ASAE American Society of gricultural Engineers, vol. 43, no.6, pp.1969-1978, 2000.

[8] Yang Y, Miao C, and Li X, "On-line conveyor belts inspection based on machine vision," Optik - International Journal for Light and Electron Optics, vol. 125, no.19, pp.5803-5807, 2014.

[9] Tahir R M, Guiyu G, and Daming S, "An Empirical Study on Retinex Methods for Low-Light Image Enhancement," Remote Sensing, vol. 14, no.18, 2022.

[10] Rongtai C, Zekun C, "Brain-like retinex: A biologically plausible retinex algorithm for low light image enhancement," Pattern Recognition, vol. 136, 2023.

[11] Jobson, Daniel J, "Retinex processing for automatic image enhancement," Electronic Imaging, vol. 13, no.1, pp100—101, 2004.

[12] Jobson D J, Rahman Z, and Woodell G A, "A multiscale retinex for bridging the gap between color images and the human observation of scenes," IEEE Transactions on Image Processing, vol. 6, no.7, pp.965-976,2002.

[13] Abràmoff M, Magalhaes P J, and Ram S J, "Image Processing Using Imagej," Biophotonics International, vol. 11, 2004.

[14] Sudsawat S, Limhengha S, "Utilizing color analysis and image processing for the assessment of the color of block para rubber," Measurement, vol. 238, pp.115344-115344,2024.

[15] Bo Y Y, Elbuken C, and Ren C L, "Image processing and classification algorithm for yeast cell morphology in a microfluidic chip," Journal of Biomedical Optics, vol. 16, no.6, 2011.

[16] Pałczyński K, Seyda J, and Skibicki D, "An image processing approach for fatigue crack identification in cellulose acetate replicas," Engineering Failure Analysis, vol. 164, pp.108663-108663,2024.

[17] Canny J F J M I O T, "Finding Edges and Lines in Images," Massachusetts Institute of Technology, 1983.

[18] Khudayer J S A, "X-Ray Lung Image Classification Using a Canny Edge Detector," Journal of Electrical and Computer Engineering, 2022.

[19] Duda R O, Hart P E, "Use of the Hough transformation to detect lines and curves in pictures," Cacm, vol. 15, no.1, pp.11-15, 1972.

[20] Wenzhu Wang, Shaochuan Xu, and Yue Teng, "Design of Belt Sprinkler Monitoring System Based on Image Processing Technology," IAENG International Journal of Computer Science, vol. 49, no.1, pp.94-100, 2022.

[21] Khaoula Slime, Abderrahim Maizate, and Larbi Hassouni, "Toward a Model to Predict Cardiovascular Disease Risk Using a Machine Learning Approach," IAENG International Journal of Computer Science, vol. 51, no. 5, pp.519-527, 2024

[22] Hadi Fattahi, Hossein Ghaedi, and Danial Jahed Armaghani, "Optimizing fracture toughness estimation for rock structures: A soft computing approach with GWO and IWO algorithms," Measurement, vol. 238, pp.115306-115306, 2024.

**WENZHU WANG** was born in Jilin Province, P. R. China, received the M.S. degree in Control Science and Engineering with University of Science and Technology Liaoning, Anshan, P. R. China, in 2023.

She is currently a Teaching assistant of School of Information Technology, Changchun Technical University of Automobile, Changchun, P. R. China. Her research interest is image processing research.

**SHAOCHUAN XU** was born in Liaoning Province, P. R. China, received the B.S. degree in automation from University of Science and Technology Liaoning, Anshan, P. R. China, received the M.S. degree in control science and engineering from University of Science and Technology Liaoning, Anshan, P. R. China, in1995, and 2004.

He is currently a professor in School of Electronic and Information Engineering, University of Science and Technology Liaoning, Anshan, P. R. China. He has authored over 30 research papers indexed by SCI and EI. His research interests include research on industrial intelligent control and machine vision.

**BO CONG** was born in Jilin Province, P. R. China, received the M.S. degree in Mechanical Engineering with Shenyang University of Technology, Shenyang, P. R. China, in 2023.

He is currently a Teaching assistant of School of Electrical Engineering, Changchun Technical University of Automobile, Changchun, P. R. China. His research interest is image processing research.